

# CD73 inhibits cGAS-STING and cooperates with CD39 to promote pancreatic cancer

Célia Jacobberger-Foissac<sup>\*1,2,3</sup>, Isabelle Cousineau<sup>\*2,3</sup>, Yacine Bareche<sup>\*1,2,3</sup>, David Allard<sup>1,2,3</sup>, Pavel Chrobak<sup>2,3</sup>, Bertrand Allard<sup>2,3</sup>, Sandra Pommey<sup>2,3</sup>, Nouredin Messaoudi<sup>4,5</sup>, Yannic McNicoll<sup>6</sup>, Geneviève Soucy<sup>7</sup>, Secil Koseoglu<sup>8</sup>, Ricard Masia<sup>8</sup>, Andrew C. Lake<sup>8</sup>, Heewon Seo<sup>9</sup>, Christopher B. Eeles<sup>9</sup>, Neha Rohatgi<sup>9</sup>, Simon C. Robson<sup>10</sup>, Simon Turcotte<sup>2,3,11</sup>, Benjamin Haibe-Kains<sup>9,12,13,14,15</sup> and John Stagg<sup>#,1,2,3</sup>

\* Contributed equally

# Correspondence: 900 St-Denis Street, Montréal, QC, Canada, H2X 0A9; john.stagg@umontreal.ca; Tel: 514-890-8000 ex:25170

## Authors' Affiliations:

1. Faculty of Pharmacy, University of Montreal.
2. Cancer Axis, Centre de Recherche Du Centre Hospitalier de l'Université de Montréal, Montreal, Quebec, Canada.
3. Institut du Cancer de Montréal.
4. Department of Surgery, University of Antwerp, Antwerp, Belgium.
5. Department of Surgery, Vrije Universiteit Brussel, Universitair Ziekenhuis Brussel and Europe Hospitals, Brussels, Belgium.
6. Surgery Department, Hôpital Jean-Talon, CIUSSS NIM, Montreal, Quebec, Canada.
7. Pathology Service, Centre Hospitalier de l'Université de Montréal, Montreal, Quebec, Canada.
8. Surface Oncology, Inc. Cambridge, Massachusetts, USA.

9. Princess Margaret Cancer Centre, University Health Network, Toronto, Ontario, Canada.

10. Center for Inflammation Research, Gastroenterology, Departments of Medicine and Anesthesia, Beth Israel Deaconess Medical Center, Harvard Medical School, Boston, MA, USA.

11. Hepatopancreatobiliary Surgery & Liver Transplantation Service, Centre Hospitalier de l'Université de Montréal, Montreal, Quebec, Canada.

12. Department of Medical Biophysics, University of Toronto, Toronto, Ontario, Canada

13. Department of Computer Science, University of Toronto, Toronto, Ontario, Canada

14. Ontario Institute for Cancer Research, Toronto, Ontario, Canada

15. Vector Institute for Artificial Intelligence, Toronto, Ontario, Canada

**Running title:** CD39 and CD73 constitute non-overlapping targets in PDAC

**Keywords:** pancreatic cancer, immunotherapy, CD39, CD73, immune checkpoint

#### **Additional information**

##### **Funding**

J.S. received research funds from the Canadian Institutes of Health Research, the Fonds de Recherche du Québec-Santé (FRQS), the Terry Fox Research Institute, the Quebec Cancer Consortium, the Chaire Jean-Guy Sabourin Research de l'Université de Montréal and Surface Oncology inc. S.T. received research funds from the FRQS and the Chaire Roger Des Groseillers en oncologie chirurgicale hépatobiliaire et pancréatique de l'Université de Montréal. SCR received research funds from the National Institute of Health (R01 DK108894; R21 CA164970 and R21 CA221702),

Tizona Therapeutics, Emerson Collective Foundation and USA Department of Defense Award (W81XWH-16-0464).

**Authors' Contributions:**

CJF, IC, DA, PC, BA, SP, NM performed histological analyses, in vitro and in vivo assays and edited the manuscript.

YB, HS, CE, NR performed bioinformatics analyses

NM, YM, GS, ST participated in sample collection and/or analysis

SK, RM ACL performed histological analyses, analyzed data and/or edited the manuscript

SCR, ST, BHK, JS funded and supervised the study, wrote and/or edited the manuscript.

**Competing Interest Statement:**

JS holds stocks, received grant support and is a Scientific Advisory Board (SAB) member of Surface Oncology Inc. JS is a SAB member of Tarus Therapeutics. SCR is a scientific founder of Purinomia Biotech Inc and consults for eGenesis, AbbVie and SynLogic Inc; his interests are reviewed and managed by HMFP, Beth Israel Deaconess Medical Center in accordance with institutional conflict-of-interest policies. ST received grant funding from Bristol-Myers Squibb, Iovance Biotherapeutics, Turnstone Biologics, and is a SAB member of Turnstone Biologics.

## Abstract

The ectonucleotidases CD39 and CD73 catalyze extracellular adenosine triphosphate (ATP) to immunosuppressive adenosine (ADO), and as such, represent potential cancer targets. We investigated biological impacts of CD39 and CD73 in pancreatic ductal adenocarcinoma (PDAC) by studying clinical samples and experimental mouse tumors. Stromal CD39 and tumoral CD73 expression significantly associated with worse survival in human PDAC samples and abolished the favorable prognostic impact associated with the presence of tumor-infiltrating CD8<sup>+</sup> T cells. In mouse transplanted KPC tumors, both CD39 and CD73 on myeloid cells, as well as CD73 on tumor cells, promoted polarization of infiltrating myeloid cells towards an M2-like phenotype, which enhanced tumor growth. CD39 on tumor-specific CD8<sup>+</sup> T cells and pancreatic stellate cells also suppressed IFN $\gamma$  production by T cells. Although therapeutic inhibition of CD39 or CD73 alone significantly delayed tumor growth *in vivo*, targeting of both ectonucleotidases exhibited markedly superior anti-tumor activity. CD73 expression on human and mouse PDAC tumor cells also protected against DNA damage induced by gemcitabine and irradiation. Accordingly, large-scale pharmacogenomic analyses of human PDAC cell lines revealed significant associations between CD73 expression and gemcitabine chemoresistance. Strikingly, increased DNA damage in CD73-deficient tumor cells associated with activation of the cGAS-STING pathway. Moreover, cGAS expression in mouse KPC tumor cells was required for anti-tumor activity of the CD73 inhibitor AB680 *in vivo*. Our study, thus, illuminates molecular mechanisms whereby CD73 and CD39 seemingly cooperate to promote PDAC progression.

## Synopsis

The clinical and biological impact of ectonucleotidases CD73 and CD39 in pancreatic adenocarcinoma (PDAC) is poorly defined. Here, complementary roles for CD73 and CD39 are revealed and uncover a novel mechanism whereby CD73 promotes immune escape in PDAC.

## Introduction

With increasing incidence and 5-year overall survival rates under 20%, pancreatic ductal adenocarcinoma (PDAC) is predicted to become the second leading cause of cancer-related death in Western countries (1,2). The vast majority of patients are diagnosed with advanced or metastatic disease, for which systemic multiagent cytotoxic chemotherapy associates with a median survival of less than a year, at the price of significant side-effects (3–5). Despite the progress of cancer immunotherapy (6), monoclonal antibodies (mAbs) targeting PD-1/L1 or CTLA-4 have shown limited efficacy against PDAC (7,8). Several mechanisms have been proposed to explain PDAC resistance to immunotherapy, such as T-cell exclusion and a predominant myeloid cell infiltration (7,9–11).

Extracellular adenosine (ADO) is an important immunosuppressive metabolite with broad effects on both innate and adaptive immune responses (12). Two ectonucleotidases play a central role in ADO accumulation: CD39, which hydrolyzes extracellular ATP into AMP, and CD73 that hydrolyzes extracellular AMP into ADO. Extracellular ADO mediates its immunosuppressive effects through activation of high-affinity A2A adenosine receptors on lymphoid and myeloid cells, and through activation of low-affinity A2B adenosine receptors on myeloid cells. A2B receptors are also often

overexpressed in cancer cells, and have been shown to promote tumor cell proliferation, metastasis, and chemoresistance through ERK, p38, JNK, AKT, and/or STAT3 signaling (13–16).

Across cancer types, ADO-producing CD73 is particularly high in PDAC (12) and correlates with poor clinical outcomes (17–20). This has prompted clinical evaluation of CD73 inhibitors, including in PDAC patients. Recently, preliminary data from early-phase clinical trials have revealed encouraging signs of clinical activity of the CD73 small-molecule inhibitor AB680 (NCT04104672) and the CD73 mAb oleclumab (NCT02503774) in PDAC patients (21,22). The clinical and biological impact of CD39 on PDAC is less well defined, albeit earlier clinical studies have revealed expression patterns of this ecto-enzyme in chronic pancreatitis and PDAC (23). By scavenging extracellular ATP, CD39 not only provides a substrate for ADO production, it also prevents activation of pro-inflammatory ATP receptors, notably P2X7 receptors (24). Because CD39 inhibitors are now being evaluated in clinical trials, it is essential to better define the relative roles of CD39 and CD73 in PDAC.

We, here, further describe CD39 to be an important factor in PDAC progression, in cooperation with CD73. CD39 expression on myeloid cells, fibroblasts, and effector T cells all contributed to the suppression of anti-tumor immunity against PDAC. Notably, our study revealed that targeting host CD39 significantly enhanced the therapeutic activity of CD73 inhibition against established tumors. Finally, we demonstrate previously unappreciated roles for tumor-associated CD73 in regulating the pro-inflammatory cGAS-STING pathway.

## Materials and Methods

### MetaGxPancreas Gene expression dataset acquisition

NT5E (*CD73*) and ENTPD1 (*CD39*) gene expression prognostic values were investigated in the curated MetaGxPancreas dataset (<http://bioconductor.org/packages/MetaGxPancreas/>) (25). Only studies with more than 40 patients were kept in the meta-analysis. RNA-Seq and clinical data from another Canadian PDAC cohort (ICGC\_CA) of 186 PDAC patients was retrieved from the International Cancer Genome Consortium (ICGC) under the accession code: PACA-CA. This resulted in 12 independent PDAC studies providing data for 1,216 patients. For each dataset, each investigated gene was scaled using the z-score method, and median gene expression was used as cutoffs in prognostic analyses.

### Gene signature

Immune gene signatures CYT (cytolytic activity)(26), CD8<sup>+</sup> T cells (27), and regulatory T cells (Tregs, *FOXP3* and *CCR8*) were computed using Gene Set Variation Analysis (GSVA) method (28).

### Pharmaco-genomic datasets

To determine whether NT5E (*CD73*) expression correlated with a distinct pattern amongst drug sensitivity profiles, we analyzed the pharmacological and expression profiles of PDAC cancer cell lines from three independent pharmaco-genomic datasets from the Bioconductor R package PharmacoGx (<http://bioconductor.org/packages/PharmacoGx>) (29): Genentech Cell Line Screening Initiative (gCSI) (30); Genomics of Drug Sensitivity in Cancer (GDSC) (31); and the

Cancer Therapeutics Response Portal (CTRP) (32). For drug sensitivity profile, C-index was computed using “paired.concordance.index.new” function from the wCI package (<https://github.com/bhklab/wCI>) derived from the survcomp package.

### **Study approval**

Our study on human PDAC samples was approved by the Research Ethics Board of the Centre Hospitalier de l'Université de Montréal. Written informed consent was acquired from all patients. Handling and breeding of mice and all experiments were performed in accordance with the Canadian laws for animal protections and were approved by the Institutional Animal Protection Committee (CIPA, CRCHUM, Montreal, Canada).

### **Patients and tissue microarrays**

Tissue microarrays (TMA) were constructed from a total of 104 consecutive patients operated on for PDAC at the Centre Hospitalier de l'Université de Montréal between February 2000 and October 2008. Formalin-fixed paraffin-embedded (FFPE) tumor blocs with adjacent non-tumoral pancreas were selected after pathology review and used to build the TMA and generate associated data. Tumors were processed by the CHUM pathology department along standard procedures for FFPE and stored at room temperature. The study was conducted in accordance to the Declaration of Helsinki after local Institutional Review Board approval. Each case was represented by three 1 mm diameter tumor cores and four 1 mm diameter cores from adjacent normal pancreatic tissue. For the serology cohort, serum from 238 patients with PDAC, 10 patients with benign hepato-biliary disease and 10 healthy volunteers were collected by the Hepatopancreatobiliary Cancer Biobank of the Centre Hospitalier de l'Université de Montréal between 2010 and 2017. None of the patients had received chemotherapy or



radiotherapy before sampling. Patient clinicopathological data, including age, gender, details of pathological diagnosis, serum CA 19–9 levels, type of surgical resection, perioperative blood loss, and overall survival (OS) were collected prospectively.

### **Automated quantitative immunofluorescence analysis**

Multicolor immunofluorescence (IF) staining of the TMAs was conducted using mouse monoclonal anti-CD73 (1/300, Ab91086; Abcam), anti-CD39 (1/500, Ab223843; Abcam), anti-CD8 (1/50, NCL-L-CD8-4B11; Leica Biosystems), in addition to anti-cytokeratin 8/18 (CK) rabbit monoclonal antibody (1/2, IR094; Dako) to reveal the epithelial areas. Briefly, TMA slides were deparaffinized and rehydrated with xylene and alcohol, followed by antigen retrieval in citrate buffer (target retrieval solution; Dako, S1699). Protein block solution (Dako, X0909; 100%) was added for 30 minutes prior to an overnight incubation at 4°C with primary antibodies. Secondary antibodies (Mouse IgG1 647 cat# A21240, Rabbit 750 cat# A21039, Mouse IgG2b 594 cat# A21145, Mouse IgG2a 488 cat# A21131; Life technologies, 1/400) were incubated for 2 hours at room temperature, followed by 4',6-diamidino-2-phenylindole (DAPI; Sigma) DNA staining and slides were mounted using ProLong Gold (ThermoFisher). The stained TMA slides were imaged at 20X magnification using the VS-110 scanner (Olympus) using 0.75NA objective and a resolution of 0.3225µm for each color channel. Images were then analyzed with Visiormorph DP image analysis software (Visiopharm), allowing automated image analysis of all cores in a batch-processed manner to ensure unbiased classification and measurement. The cores areas were defined using DAPI staining. Epithelial areas stained positive for CK. Stromal area was determined to be the core area minus the epithelial area. All images were visually reviewed to remove staining artifacts and damaged tissue areas prior to further analysis. CD73 and CD39 expression were

defined by mean fluorescence intensity (MFI). MFI were calculated as the mean of CD73 or CD39 fluorescence intensity per pixel per compartment: epithelium, stroma, or total core area. Upper tertiles of CD73 or CD39 MFI were used as cut-offs. The number of CD8<sup>+</sup> T cells were counted using Visiormorph DP software. The CD8 density represents the number of CD8<sup>+</sup> T cells divided by the surface area (CD8/cm<sup>2</sup>). For each patient, CD73 or CD39 mean fluorescent intensity (MFI), or CD8 density values of replicates' core area were calculated, and the mean of replicates was used for prognostic evaluation. The endpoint for the study was OS. OS was defined as the time from surgery to death or censoring.

### **Animals and cell lines**

All animal studies were conducted in accordance with, and with the approval of, the Institutional Animal Care and Use Committee (IACUC) of the CRCHUM. C57BL/6 (B6) mice were purchased from Charles River Laboratories, LysMCre<sup>+/-</sup> and OT-I B6 mice were from Jackson Laboratories, and CD73 flox/flox B6 mice were from Cyagen (33). The global CD39<sup>-/-</sup> and CD39<sup>fl/fl</sup> BL6 mice were provided by Simon C. Robson (34,35). LysMCre<sup>+/-</sup> CD73<sup>fl/fl</sup>, LysMCre<sup>+/-</sup> CD39<sup>fl/fl</sup>, and OT-I CD39<sup>-/-</sup> mice were generated by crossing respective parental strains and maintained at the CRCHUM animal house, Montreal, Canada.

KPC 1245 and KPC 1199 cells (KPC cells) derived from David Tuveson's laboratory (Cold Spring Harbor laboratory) were a gift from Tracy L. McGaha (Princess Margaret Cancer Centre, Toronto) and were obtained in 2019. PANC1 cells were purchased from ATCC in 2019 and were not re-authenticated. All cells were maintained in complete

RPME media (10% fetal bovine serum (FBS; Wisent), no antibiotics) and tested biweekly for mycoplasma (ThermoFisher, cat# M7006).

KPC and PANC1 cells were transiently transfected by electroporation with a CRISPR-Cas9 vector (pX330; Addgene) expressing single guide (sg)RNA to mouse CD73 (5'-GCAGGATCGTGAGCTCCC-3' and 5'GCGCAAACATTAAGGCAC-3') or human CD73 (5'-GACGCCGGCGACCAAGTACCA-3' and 5'-GCAGCACGTTGGGTTCGGCG-3') provided by Michael Hoelzel (University of Bonn, Bonn, Germany). Cells were then sorted (following CD73 staining with mAb clone TY/11.8- PE-Cy7; eBioscience) using a BD FACS-Aria III to obtain a CD73-negative and a CD73-positive population (>10% of the transfected cells were negative for CD73 prior to sorting; purity > 95% after sorting). No expression of Cas9 was detected by western blot following sorting. To generate ovalbumin (OVA)-expressing cells, lentiviral vectors were produced by transfecting 293FT cells (ThermoFisher) with an OVA plasmid (#72263; Addgene) and ViraPower™ Packaging Mix (ThermoFisher Catalog #K4975-0). Supernatant was collected after 72 hours to transduce KPC1245 cells followed by FACS cell sorting based on Green Fluorescent Protein (GFP) expression (purity > 95% after sorting). All cells were used within 10 *in vitro* passages after sorting. Where indicated, CD73-positive KPC cells were transfected with CRISPR-Cas9 vector alone (Addgene; pSpCas9(BB)-2A-Puro (PX459) V2.0) or in combination with sgRNA targeting mouse cGAS (GeneScript, SC1678; sequence 5'ATATTCTTGTAGCTCAATCC-3'). Individual clones were selected and characterized for loss of cGAS expression and activity, as described. CD73-negative KPC cells were infected with a lentiviral vector (pLenti-GIII-CMV) expressing mouse Nt5e (ABM good, cat.: 322320640195) and selected in complete RMPI media (10 FBS, no antibiotics) with 1 µg/mL of puromycin (Thermo Fisher)-containing media. Surviving

cGAS-deleted cells were further enriched by FACS for the presence or absence of CD73 expression (as indicated above; purity >95%). Where indicated, CD73-positive KPC cells were infected with a lentivirus containing either one of 5 predesigned shRNAs (TRCN0000176706, TRCN0000177514, TRCN0000178625, TRCN0000178459, TRCN0000416658) or a control shGFP plasmid (all from Sigma) and selected with 1 µg/mL of puromycin-containing media. Knockdown was validated by western blot for cGAS protein expression and ELISA for cGAMP production as described.

### **ELISAs**

ELISAs were performed on serum samples from 238 patients with PDAC, 10 patients with benign hepato-biliary disease and 10 healthy volunteers. Nunc maxisorp plates (Sigma) were coated overnight with 1 µg/mL of anti-human CD73 (clone AD2, BioLegend, 344002). Blocking was done for 1 hour at room temperature in PBS, 0.01% Tween-20 (ThermoFisher), 0.1% BSA (ThermoFisher). Patient sera were incubated 2 hours at room temperature, at 100 µL per well, undiluted. Detection antibody (anti-CD73 clone 1E9, Santa Cruz, sc-32299, 5 µg/mL) was incubated for 1 hour. HRP-conjugated anti-mouse IgG3 detection antibody (1:4000 dilution; Southern Biotech 1101-05) was added for 1 hour at room temperature, followed by tetramethylbenzidine (TMB; ThermoFisher) substrate. The reaction was stopped with 2N hydrochloric acid (HCl). Absorbance was read at 450 nm and corrected at 570 nm on a Versamax microplate reader. All steps were separated by three washes with PBS, 0.01% Tween-20. Samples were run in duplicate or triplicate. On each plate, a standard curve of recombinant human CD73 protein (R&D Systems, 5795-EN) was run. For the 2'3'-cGAMP ELISA, KPC cells were cultured in DMEM with 10% FBS containing 20 nM gemcitabine for 48

hours ( $10^6$  cells per well of a 6-well plate, in 700 $\mu$ L), and the undiluted supernatant harvested and used in a commercial 2'3'-cGAMP ELISA kit following manufacturer's instructions (Cayman chemical, 501700). Where indicated, cells were treated with 1.5  $\mu$ g/mL dsDNA consisting of a PCR product (0.7 kb in length) from an irrelevant plasmid (Addgene cat#125570). The PCR product was purified using QIAGEN DNA purification kit (QIAGEN, Cat.: 28104) and quantified on a nanodrop (DeNovix) instrument. The PCR product was mixed with OPTI-MEM media (Gibco, Cat.: 31985070) containing 1X Lipofectamine 2000 (ThermoFisher, Cat.: 11668030) and added to cells (300 $\mu$ L per well). Cells were incubated for 8hrs at 37°C and supernatant was harvested and analyzed undiluted for 2'3'-cGAMP levels by ELISA (Cayman Chemical, Cat.: 501700).

### **Western blots**

Adherent cells were washed with ice-cold PBS and lysed and scrapped in CelLytic™ M buffer (Sigma) with 1X Halt™ protease and phosphatase cocktail inhibitors (Thermo Fisher) before being centrifuged for 15 minutes at 20,000 x *g* at 4°C. Proteins were harvested from supernatant and quantified by using Bradford protein assay dye reagent (Bio-Rad). 25  $\mu$ g of protein from whole cell extract were loaded in 4-10% acrylamide gels and transferred on nitrocellulose membranes. Membranes were stained overnight in 5% BSA-containing PBS Tween 0.1% with following antibodies: mouse anti-PLC $\gamma$  (1:2000; Millipore #05-163) and rabbit anti-cGAS (mouse; 1:1000; Cell signaling #31659). Proteins were revealed with fluorescent secondary anti-rabbit (1:10000; LI-COR #926-68073) or anti-mouse antibodies (1:10000; LI-COR #926-32212) using the LI-COR fluorescent scanner.

### ***In vivo* experiments**

KPC cells ( $5 \times 10^5$ ) were injected subcutaneously (s.c.) into indicated strains of female C57BL/6 mice. On indicated days, mice were treated with gemcitabine (100 mg/kg, i.p.), anti-mouse CD39 mAb (clone VX26102) or control Ig (400  $\mu$ g i.p.) (Supplementary Table S1, "In vivo"), or AB680 (MedChem Express; 10 mg/kg s.c. peri-tumoral). Tumor growth was monitored using calipers three times per week. Tumors were harvested for real-time PCR or for tumor-infiltrating lymphocyte (TIL) analysis on days 11 or 12 after implantation as described below. In some experiments, disease-free survival was determined as the day when the tumor size reached 50 mm<sup>2</sup>.

### CD39 IHC analysis

Subcutaneous KPC tumors from CD39<sup>fl/fl</sup> LysMCre<sup>+/-</sup> and CD39<sup>fl/fl</sup> LysMCre<sup>-/-</sup> mice collected at the indicated endpoints were formalin-fixed, paraffin-embedded, and sectioned into 5-micron sections for immunohistochemistry (IHC) and tumor area measurement. Dewaxing, antigen retrieval, and staining were performed in a Leica Bond Rx automated stainer (Leica Biosystems). For CD39 staining, slides were exposed to ER1 solution (Leica cat# AR9961) for 10 minutes at 100°C, followed by a 1-hour incubation with rabbit monoclonal anti-mouse CD39 (Cell Signaling Technology, clone E2X6B, CST #14481) at room temperature at 1:100 dilution. Slides were dehydrated and cover-slipped and were digitally scanned in an Aperio Versa 200 scanner (Leica Biosystems). CD39 staining and tumor area were quantitated on digitally scanned slides using the Area Quantification module in HALO v3 (Indica Labs) after the tumor was manually outlined as the region of interest. Data are expressed as CD39 IHC H-index. The H-index is equal to the percentage of tissue positive for a given marker multiplied by the average optical density of tissue positive for that marker. Tumor area is expressed as mm<sup>2</sup>.

### **FACS analysis of tumor-infiltrating lymphocytes**

Tumors were excised, cut with scissors, and were subsequently incubated with a solution composed of 1 mg/mL collagenase IV (Sigma) and 0.02 mg/mL DNase I (Sigma) in serum-free RPMI medium for 45 min at 37°C on a heating rotating plate (190 rpm). Cell suspensions were filtered using a 40 µm cell strainer and washed with 20 mL cold FACS buffer (PBS 2% FBS, 5mM EDTA). Cells were centrifuged at 300g for 5 min, and resuspend in cold FACS Buffer, filter through 5 mL round-bottom polystyrene test tubes with cell strainer cap (ThermoFisher) and kept on ice until transfer into 96 U-bottom plates (ThermoFisher) for staining. Following Fc block (anti-CD16/32 mAb (BD Bioscience) for 10 minutes at 4°C), antibodies against cell surface antigens were added (30 minutes incubation at 4°C). For staining of intracellular antigens cells were fixed, permeabilized (eBioscience FoxP3/Transcription Factor Staining Buffer Set) and stained with antibodies following manufacturer's provided protocol (Supplementary Table S1, "FACS antibodies"). FMO controls were always included as negative controls. To detect OVA-specific CD8<sup>+</sup> T cells, we used OVA257-264 (SIINFEKL) peptide bound to H-2Kb monoclonal antibody (eBio25-D1.16 (25-D1.16))-APC (from eBioscience, cat #17-5743-82). Flow cytometry was performed on BD LSR Fortessa (BD Bioscience), and FlowJo software was used for analysis.

### **Quantitative real-time PCR**

RNA from homogenized mouse tumor tissue or cell pellets from cGAS-targeted cells, was isolated using RNAeasy Mini Kit (Qiagen) according to manufacturer supplied protocol. Synthesis of cDNA was done using the Superscript VILO cDNA Synthesis Kit (Invitrogen). Real-time PCR was performed using TaqMan probes (Supplementary Table

S1, “Real-time TaqMan”) and TaqMan Fast Advanced Master Mix (ThermoFisher) on the Step One Plus Thermal Cycler. For template, 1µg of RNA was used for reverse transcription. Resulting cDNA was diluted 1/10 in ddH<sub>2</sub>O which accounts for 100 ng RNA per reaction. Analysis of each gene per samples was run in triplicate. Beta-actin (Actb; probe Mm00607939\_s1; ThermoFisher) was used as endogenous control. Relative quantification was measured by  $2^{-\Delta\Delta CT}$  (computed by StepOne software; ThermoFisher).

### **Spheroid formation and OT-I activation assay**

Wild-type (WT) and CD39<sup>-/-</sup> OT-I cells were obtained from splenocyte single-cell suspensions. CD8<sup>+</sup> T cells were purified (>90%) by immunomagnetic negative selection (Stem cell EasySep™ 19853). CD8<sup>+</sup> T cells, at 1 x 10<sup>6</sup> cells per mL, were stimulated for 4 days using plate-bound anti-CD3 (0.5 µg/mL; BioXCell cat.: BE0001-1), soluble anti-CD28 (5 µg/mL; BioXCell cat.: BE0015-1), recombinant IL2 (30 U/mL; CHUM Pharmacy), and recombinant IL7 (0.5 ng/mL; R&D System Cat.: 407-ML-005). To isolate primary pancreatic stellate cells, mouse pancreas were harvested and minced under sterile conditions and transferred into gelatin (Fisher Scientific, Cat.:G7-500)-coated (0.2% in H<sub>2</sub>O for 2hrs at 37°C) petri dishes in DMEM/F12 (Wisent, Cat.: 319-075-CL) media containing 20% FBS, 100IU Penicillin and 100µg/mL streptomycin (Wisent, Cat.: 450-201-EL), 10µg/mL gentamycin (Wisent, Cat.: 450-135-XL), 10mM HEPES (Wisent, Cat.: 330-050-EL), 1% glutamax (Gibco, Cat.: 35050061), 1% MEM nonessential amino acids (Wisent, Cat.: 321-011-EL), 1mM sodium pyruvate (Wisent, Cat.: 600-110-EL) and 20ng/mL of basic Fibroblast Growth Factor (bFGF) (PeproTech, cat.: 450-33). Gentamycin and bFGF were removed from culture after 3 passages. The ratio of KPC (1000 cells), stellate (1000 cells) and OT-1 (10 000 cells) was 1:1:10.



Spheroids were formed by seeding 1,000 KPC cells per well into round bottom, non-tissue culture-treated 96 well-plates in 100  $\mu$ L DMEM (Wisent, Cat.: 319-005-CL) containing 10% FBS and supplemented with 0.24% methyl cellulose (Sigma). Spheroids were allowed to form for 24 hours prior to use in assays (36). For some conditions, 500 primary pancreatic stellate cells purified from CD39<sup>-/-</sup> or WT mice were mixed with the KPC cells during the spheroid formation. OT-I CD8<sup>+</sup> T cells were added to the spheroid at an effector:target (E:T) ratio of 10:1.. After 4 hours, a protein transporter inhibitor cocktail was added (ThermoFisher 00-4980-03) for another 4 hours of incubation. Supernatants (100  $\mu$ l, undiluted) were harvested and IFN- $\gamma$  production was measured by ELISA (R&D system, DY485-05) following manufacturer instructions. Spheroids were harvested, dissociated with trypsin (Sigma), and stained with Thy1.2, IFN $\gamma$ , and viability dye (Supplementary Table S1, "FACS antibodies") for FACS analysis of IFN $\gamma$  production. Flow cytometry was performed on BD Fortessa (BD Bioscience), and FlowJoFlow Jo software was used for analysis.

### ***In vitro* proliferation assay**

For evaluation of cell proliferation, KPC and PANC1 cells were seeded in 96-well plates. After overnight adhesion, 15 nM of gemcitabine was added. Cell number was imaged using phase-contrast microscopy. Images were captured using the IncuCyte<sup>TM</sup> Live-Cell Imaging System (Incucyte HD). Proliferation curves were generated based on measurement of proportion of confluence using the IncuCyte software. In addition, cells were seeded in 96-well plates, and gemcitabine was added 24 hours later at various concentrations. After 72 hours of treatment, the number of viable cells was detected using CellTiter-Glo luminescent viability kit (Promega) using TopCount NXT microplate scintillation and luminescence counter (PerkinElmer). Data are represented as a ratio of

relative luminescence (RLU) following treatment with gemcitabine over RLU without treatment.

### **$\gamma$ -H2AX immunofluorescence (IF)**

Cell lines were seeded on glass-cover slips, allowed to attach for 24 hours, and then treated for 48 hours with gemcitabine, radiation (1Gy using Gammacell® 3000 irradiator Elan), BAY 60-6583 (1 $\mu$ M; Tocris, cat #4472). or AB680 (0.1 $\mu$ M; MedChem Express, cat #2105904-82-1). Cells were fixed 10 minutes with 10% formalin and permeabilized 15 minutes with PBS, 0.25% Triton-X100 (Sigma). Unspecific binding sites were blocked for 1 hour using PBS, 1% BSA, 4% goat serum (ThermoFisher). Primary antibody against  $\gamma$ H2AX (Milipore, JBW301, 1/2000) was incubated overnight at 4°C. Goat anti-mouse antibody coupled with Alexa Fluor-647 was incubated for 1 hour at room temperature (1/400 dilution), followed by DAPI staining. Cover slips were mounted on glass slides and imaged at 40X magnification with a VS-110 scanner (Olympus). Images were then analyzed with Visiomorph DP image analysis software (VIS, Visiopharm) allowing automated nucleus and  $\gamma$ H2AX foci count following a sequential process. DAPI counterstaining was used for nuclei identification, and for each nucleus, the number of  $\gamma$ H2AX foci was calculated. For each replicate, at least 20 nuclei are analyzed and each condition was tested in triplicate.

### **Statistical analysis**

The Kaplan-Meier method was used to estimate survival rates, and the log-rank test was used to assess survival differences between groups. The Cox proportional hazards model for multivariate survival analysis (forward conditional) was used to assess univariate predictors related to OS. The SPSS software program (version 24.0; IBM

Corporation) was used for statistical analysis. Graphical representations were performed with GraphPad Prism 7 (San Diego, CA) software. Differences between two continuous variables were assessed using Wilcoxon rank sum test. Spearman correlation was used to investigate association between gene expression and immune gene signature. Association of specific biomarkers survival was assessed using Cox proportional hazard model to assess the discrimination or separation of a survival model. Meta-analysis was performed to improve result reproducibility. Each individual independent study was investigated separately, and then statistical results were pooled using random-effects meta-analysis with inverse variance weighting in DerSimonian and Laird random-effects models (37). Heterogeneity across studies was evaluated by using the Q statistic along with index, which describes the total variation across studies attributable to heterogeneity rather than sampling error (38). Note that values greater than 50% along with Cochran's Q statistic represent moderate to high heterogeneity (37). All analyses were performed on the R platform (version 4.1.0). Associations were deemed statistically significant for p-values lower or equal to 0.05.

For mouse studies, we used Wilcoxon rank-test or unpaired t-test to compare two groups and one-way ANOVA or multiple t-tests to compare multiple groups. Recommended *post-hoc* multiple comparison tests were used when required. Outliers were identified using the ROUT method. Analyses were performed using GraphPad Prism version 9.1.0. The statistical tests used to calculate P values are noted in the figure legends. \*  $p < 0.05$ , \*\*  $p < 0.01$ , \*\*\*  $p < 0.001$ , ns: not significant.

### Data availability

The code for analysis scripts is publicly available in Github at [https://github.com/barechey/PDAC\\_CD73\\_and\\_CD39](https://github.com/barechey/PDAC_CD73_and_CD39). The remaining data generated in this study are available upon request from the corresponding author.

### **Research reproducibility**

A complete software environment through CodeOcean containing the pharmacogenomic analysis, necessary data, and code to reproduce the pharmacogenomic analysis and figures described in this manuscript is available at: <https://codeocean.com/capsule/3210626/tree/v1> (DOI: 10.24433/CO.5854848.v1)

## **Results**

### **Tumoral CD73 and stromal CD39 are both associated with poor PDAC survival**

To investigate the prognostic impact of the adenosine pathway in PDAC, we initially performed a gene expression meta-analysis of CD73 and CD39 in 12 curated independent studies encompassing over 1,200 PDAC patients. CD73 was significantly associated with worse overall survival (OS) (Fig. 1A). CD39 overall was linked to better OS (Suppl. Fig. S1A), although this did not reach statistical significance in individual cohorts (Suppl. Fig. S1B-C). We next explored the prognostic association between CD73 and CD39 in the two largest cohorts (i.e., TCGA and ICGC). The CD73 association with a worse prognosis was only observed when PDAC tumors had concomitant high CD39 expression (Fig. 1B, Suppl. Fig. S1D). Correlative analyses in the two largest cohorts further revealed a significant positive correlation between CD39 gene expression and markers of cytotoxic T cells, Tregs, and T-cell exhaustion (i.e.,

*PDCD1*, *CTLA4*, *TIGIT*, *LAG3*), whereas CD73 showed no significant correlations (Fig. 1C, Suppl. Fig. S1E).

We next investigated the histological distribution of CD73 (Fig. 2A) and CD39 (Fig. 2B) protein expression in the epithelium and stroma of PDAC surgical samples from an independent cohort (Suppl. Table S2). Compared to matched normal adjacent pancreatic tissue, CD73 was significantly upregulated in the PDAC tumor epithelium and weakly, but significantly, downregulated in the tumor stroma (Fig. 2C). CD39, on the other hand, was significantly upregulated in the stroma of PDAC tumors (Fig. 2D). A significant association was observed between tumor epithelial CD73 and higher stage and poorly differentiated PDAC tumors, whereas no correlation was observed between CD39 and available clinicopathological characteristics (Suppl. Table S3).

Survival analyses revealed that higher tumor epithelial CD73 expression (Fig. 2E), as well as higher tumor stromal CD39 expression (Fig. 2F), associated with worse OS of PDAC patients (Table 1). Tumor epithelial CD73 expression associated with worse OS in multivariate analyses when adjusting for pre-operative CA 19-9, nodal status, differentiation, and resection margin (Table 1). Survival analyses combining epithelial CD73 and stromal CD39 expression provided further prognostication (Suppl. Fig. S2A).

### **CD73 and CD39 abolish the good prognostic impact of tumor-infiltrating CD8<sup>+</sup> T cells**

As previously shown in other PDAC cohorts (39,40), the presence of tumor-infiltrating CD8<sup>+</sup> T cells associated with improved OS (Suppl. Fig. S2B). Supporting our gene expression data (Fig. 1C), CD39 protein expression positively correlated with CD8<sup>+</sup> T-cell infiltration (Suppl. Fig. S2C), whereas CD73 protein expression was not correlated

with tumor-infiltrating CD8<sup>+</sup> T cells (Suppl. Fig. S2D). We next investigated whether CD73 or CD39 expression impacted PDAC immunosurveillance. High expression of tumor epithelial CD73 (Fig. 2G) or tumor stromal CD39 (Fig. 2H) completely abrogated the good prognostic value of tumor-infiltrating CD8<sup>+</sup> T cells in PDAC patients.

### **Soluble CD73 associates with worse PDAC survival**

Because CD73 can be cleaved from the cell surface and found in soluble form, we next evaluated whether soluble CD73 (sCD73) could serve as a non-invasive prognostic biomarker of PDAC. In an independent cohort (Suppl. Table S2), we observed that sCD73 was significantly higher in patients with benign or malignant pancreatic tumors compared to healthy donors (Fig. 2I, Suppl. Fig. S2E). Higher sCD73 in PDAC patients associated with higher CA 19-9 levels, tumors located in the head of the pancreas, higher stage, and lymphovascular invasion (Suppl. Table S3). Higher sCD73 also significantly associated with worse OS (Fig. 2J). In multivariate analysis, however, sCD73 did not reach significance (Table 1). We next assessed whether sCD73 in serum could be used as a surrogate of CD73 expression in PDAC tumors. In a sub-cohort, no correlation was observed between soluble and tumoral CD73 levels (Suppl. Fig. S2F).

### **CD73 on tumor cells and myeloid cells favors infiltration of M2-like myeloid cells in murine PDAC**

We next investigated the role of tumor-derived CD73 using Crispr/Cas9-mediated gene deletion in mouse KPC or human PANC1 tumor cell lines (Suppl. Fig. S3A). KPC and PANC1 were negative for CD39 expression (Suppl. Fig. S3B). *In vitro*, tumor-derived CD73 had no impact on tumor cell proliferation (Suppl. Fig. S3C). However, loss of tumor-derived CD73 significantly decreased KPC tumor growth *in vivo* and improved

gemcitabine activity (Fig. 3A). This associated with a significant increase in tumor IFN $\gamma$  levels and a weak, but significant, increase in IL10 and arginase-1 (Fig. 3B). Deletion of tumor-derived CD73 also significantly decreased infiltration and polarization of M2-like tumor-associated macrophages (TAMs) and monocytic myeloid-derived suppressor cells (M-MDSCs) in KPC tumors (Fig. 3C, Suppl. Fig. S3D). Targeting tumor-derived CD73 had no impact, however, on CD8, CD4, or granulocytic (G)-MDSC infiltration (Suppl. Fig. S3D; gating strategies and representative plots in Suppl. Fig. S4). Because CD73 was expressed on KPC-infiltrating myeloid cells (Suppl. Fig. S5A), we next evaluated the role of myeloid-derived CD73. Conditional CD73<sup>fl/fl</sup> mice were crossed with LysMCre<sup>+/-</sup> mice (myeloid-specific deletion of CD73) and challenged with CD73-negative KPC tumor cells. Myeloid-derived CD73 significantly enhanced KPC tumor growth (Fig. 3D), promoted infiltration of M2-like TAMs (Fig. 3E), and M2 polarization (Suppl. Fig S5B). Myeloid-derived CD73 had no impact on tumor-infiltrating CD8, CD4, M-MDSCs, or G-MDSCs (Suppl. Fig. S5C).

### **CD39 on myeloid cells, fibroblasts, and T cells suppresses anti-PDAC immune responses**

We next investigated the role of CD39. Because myeloid cells were a major source of CD39 in KPC tumors (Suppl. Fig. S6A), we assessed the impact of myeloid-derived CD39 in conditional CD39<sup>fl/fl</sup> LysMCre<sup>+/-</sup> mice challenged with KPC tumor cells. CD39 deletion in myeloid cells significantly decreased KPC tumor growth (Fig. 4A, Suppl. Fig. S6B) and significantly decreased M2-like TAM infiltration (Fig. 4B). In contrast to what we observed for CD73 (Suppl. Fig. S5C), myeloid-specific deletion of CD39 additionally associated with a significant increase in tumor-infiltrating CD8<sup>+</sup> T cells and CD4<sup>+</sup>Foxp3<sup>-</sup> T cells (Fig. 4C).

We then evaluated the role of CD39 on tumor-associated fibroblasts and effector CD8<sup>+</sup> T cells. For this purpose, we measured T-cell function using *in vitro* spheroid cultures composed of ovalbumin (ova)-expressing KPC tumor cells, primary pancreatic stellate cells (WT or CD39<sup>-/-</sup>), and ova-specific CD8<sup>+</sup> OT-I cells (WT or CD39<sup>-/-</sup>) (Fig. 4D). CD39<sup>-/-</sup> OT-I CD8<sup>+</sup> T cells, as well as CD39<sup>-/-</sup> pancreatic stellate fibroblasts, each significantly increased IFN $\gamma$  production by OT-I effector T cells (Fig. 4D).

### **Targeting CD39 and CD73 enhances gemcitabine activity against mouse PDAC**

We next evaluated whether CD39 represented a therapeutic target against PDAC. Mice with established KPC tumors (> 25 mm<sup>2</sup>) were treated with a blocking monoclonal anti-mouse CD39 three times per week from day 7, alone or in combination with gemcitabine (100 mg/kg on day 7 and 10). Anti-CD39 monotherapy significantly delayed KPC tumor growth and significantly enhanced gemcitabine activity against established tumors (Fig. 4E). Similarly, treatment with a selective CD73 inhibitor (i.e., AB680) also significantly inhibited KPC tumor growth and enhanced gemcitabine activity (Fig. 4F, Suppl. Fig. S6C).

We then evaluated whether CD39 and CD73 had redundant protumorigenic effects. For this purpose, KPC tumors were injected into WT and CD39<sup>-/-</sup> mice and treated with the CD73 inhibitor AB680 in combination with gemcitabine. Targeting host-derived CD39 further enhanced the therapeutic activity of CD73 inhibition when combined with gemcitabine (Fig. 4G). Similar results were obtained using a different KPC model (i.e., KPC 1199 cells; Suppl. Fig. S6D). Immune profiling of KPC-ova tumors treated with AB680, monoclonal anti-CD39, or both revealed that only the combined inhibition of CD73 and CD39 significantly increased tumor-specific T-cell infiltration and prevented



acquisition of the PD-1 exhaustion marker (Fig. 4H). Taken together, our results revealed non-redundant roles for CD73 and CD39 in promoting PDAC.

### **Tumor-derived CD73 protects against DNA damage and inhibits cGAS-STING**

Because PDAC cells expressed high CD73, but not CD39 (Suppl. Fig. S3A-B), we next investigated whether CD73 conferred a proliferative advantage to PDAC tumor cells in a cell-autonomous manner. As mentioned above, CD73 gene-silencing had no impact on the survival or proliferation of mouse or human PDAC cells in normal culture conditions. CD73-deletion in KPC or PANC1 cells, however, significantly enhanced tumor cell sensitivity to gemcitabine *in vitro* (Fig. 5A-B). To further evaluate the role of CD73 in PDAC chemoresistance, we next determined whether CD73 gene expression was associated with gemcitabine sensitivity in the three largest pharmacogenomics drug screening studies (i.e., Cancer Therapeutics Response Portal, Genomics of Drug Screening in Cancer, Genentech Cell line Screening Initiative). Meta-analysis of the three datasets revealed a significant inverse correlation between CD73 gene expression in PDAC cell lines and gemcitabine response (C-index=0.62,  $p<0.001$ ; Fig. 5C), as measured by the area above the drug dose-response curve. Consistent with these results, gemcitabine treatment of CD73-deficient KPC tumor cells induced significantly greater DNA damage, revealed by  $\gamma$ H2AX staining (Fig. 5D-E). Partial rescue of CD73 expression reverted phenotype and reduced DNA damage (Suppl. Fig. S7). Similar results were obtained in response to irradiation (Fig. 5F) and in human PANC1 tumor cells treated with the CD73 inhibitor AB680 (Fig. 5G). Activating A2B receptors with a selective agonist (BAY 60-6583) restored this phenotype, as revealed by a significant decrease in DNA damage in gemcitabine-treated PANC1 after A2B receptor activation (Fig. 5G) and KPC cells (Fig. 5H).

The DNA sensor cGAS can link DNA damage to inflammation through production of cyclic GMP-AMP (cGAMP), which in turn activates STING-dependent gene transcription (41). Because CD73 expression protected PDAC cells against DNA damage, we investigated whether CD73 could inhibit cGAS-STING activation. Indeed, we observed that CD73-deficient KPC cells produced significantly greater cGAMP (Fig. 5I) and expressed significantly higher STING target genes (Fig. 5J) compared to CD73-proficient tumor cells following gemcitabine treatment. This suggested a possible role for the cGAS-STING pathway in the therapeutic activity of CD73 inhibition. To test this, we deleted cGAS from parental KPC cells by Crispr/Cas9, generated a polyclonal population consisting of individual clones with confirmed loss of cGAS-STING activation (Suppl. Fig. S8), and evaluated the therapeutic activity of AB680 against cGAS-null KPC tumors and control Cas9-expressing KPC tumors. cGAS-deletion in tumor cells abrogated the *in vivo* activity of AB680 (Fig. 5K). Similar results were obtained using shRNA-based knockdown of cGAS (Suppl. Fig. S9). Taken together, our data highlights a previously unappreciated role for CD73 in regulating the cGAS-STING pathway and underscores the importance of tumor cGAS activation for therapeutic activity of CD73 inhibitors.

## Discussion

PDAC is one of the most lethal and challenging cancers. Poor clinical outcomes reflect the difficulty of early diagnosis and lack of biomarkers, high propensity to rapidly disseminate, and limited treatment options (1–3). Our study demonstrates that CD39 and CD73 ectonucleotidases not only represent prognostic biomarkers in PDAC, but that these also constitute valid and non-overlapping therapeutic targets.

In multivariate survival analyses, CD73 expression on PDAC tumor cells, measured using standard histological techniques, was found to be the most significant prognostic biomarker of overall survival (HR: 2.27; P=0.003), even after correction for positive lymph nodes, grade of differentiation, resection margins, and preoperative CA 19-9 levels. The prognostic value of intratumoral CD73 was independent and stronger than CD8<sup>+</sup> T cells. Validation of this finding could have a major impact in patient care, as preoperative serum CA 19-9 levels remains the only biomarker currently used for PDAC prognostication, despite low sensitivity and specificity, and the absence of CA 19-9 expression in 5-10% of the population (42).

High levels of soluble CD73 in serum of PDAC patients at the time of surgery also significantly correlated with worse overall survival. Serum sCD73 levels, however, lost prognostic value in multivariate analysis when combined with other pathological indicators. Our observed correlation between sCD73 and PDAC progression is in agreement with reports from Rittman et al. and Turiello et al. (43,44). In matched samples, we did not observe any correlation between sCD73 levels and tumor CD73 expression in PDAC patients. We also previously had not found any correlation in colorectal cancer patients (45). As a GPI-anchored protein, CD73 cleavage from the cell membrane can occur from the activity of metalloproteinases and cell-associated phospholipases (46–49). Upregulation of serum sCD73 in cancer patients may reflect cleavage from CD73-expressing cells outside the TME, such as lymphocytes or endothelial cells. Taken together, determining CD73 expression on PDAC tumors cells appears a better strategy for PDAC prognostication.

CD39 protein expression was significantly upregulated in PDAC stroma compared to matched normal stroma. This specific upregulation of CD39 in stroma associated with

poor patient survival and suppressed tumor immune surveillance (i.e., associated with the loss of prognostic impact of CD8-infiltrating cells). We further demonstrated that CD39 expression by primary mouse pancreatic stellate cells, the main cell type in PDAC stroma, significantly suppressed tumor-specific CD8<sup>+</sup> T-cell responses against pancreatic tumor cells.

Prior work has noted high expression of CD39 and CD39L1, together with P2R (P2X7, P2Y2, and P2Y6), in chronic pancreatitis and PDAC (35). Interestingly, CD39 expression has also been shown to promote fibrogenesis in experimental pancreatitis, likely by generation of extracellular adenosine; of potential relevance to desmoplastic PDAC responses. Indeed, CD39-deficient mice show heightened IFN $\gamma$  in response to induction of experimental pancreatitis with less generation of matrix (23).

In the transplantable KPC mouse model of PDAC, we found that CD39 expression on myeloid cells, as well as CD73 expression on tumor cells and myeloid cells, promoted infiltration of M2-like macrophages. The immune regulatory effects of CD39 on myeloid cells were non-redundant to those of CD73 expression on the same cells. Indeed, only myeloid-derived CD39, but not myeloid-derived CD73, significantly repressed T-cell infiltration in KPC tumors. Further in support of non-redundant functions for CD39 and CD73 in PDAC, targeting host CD39 added to the therapeutic activity of CD73 inhibition against KPC tumors.

Our data support previous studies demonstrating a distinctive mechanism for CD39 amongst the adenosinergic axis. Accordingly, CD39 activity not only provides the nucleoside monophosphate substrate for CD73-mediated ADO production, this

ectonucleotidase also inhibits pro-inflammatory signaling through ATP receptors such as NLRP3 inflammasome-activating P2X7 receptors. Hence, activation of the P2X7-NLRP3 pathway has been shown to be involved in the response to CD39 mAb therapy in mice (50,51). Interestingly, single-cell transcriptome analysis of infiltrating leukocytes in CT26 tumors reveals an upregulation of T-cell chemoattracting genes following treatment with CD39 mAb (52). Hence, activation of NLRP3 in response to CD39 inhibition likely contributes to promote T-cell recruitment by enhancing production of T-cell chemoattracting chemokines (53). In human PDAC, elevated NLRP3 activation has been associated with increased expression of T cell-attracting chemokines (CXCL9, CXCL10, CCL4 and CCL5) (54).

In addition to the dual impact of maintaining pro-inflammatory ATP signaling and abrogating ADO signaling, co-blockade of CD39 and CD73 may also prevent potential compensatory mechanisms, for instance those mediated through CD38 and ENPP1 (12). Because ADO can also be produced independently of CD73 or released from the intracellular pool, it would be of interest to further assess the therapeutic activity of combining anti-CD39 with an A2A and/or A2B receptor antagonists.

Interestingly, CD73 has also been shown to have immune-independent and ADO-independent functions. This is supported by observations that “catalytically dead” CD73 can promote cell survival and interactions with extracellular matrix proteins, and that targeted blockade of CD73 can delay human tumor xenografts in severely immunodeficient mice (55,56). Yet, the underlying mechanisms remain poorly defined. A recent study suggests that intracellular CD73 can enhance AKT signaling in PDAC tumor cells independently of ecto-enzymatic activity, which in turn confer resistance to gemcitabine (57). In the current study, we observed that CD73 deletion in human or

mouse PDAC sensitized tumor cells to gemcitabine *in vitro*. Blocking CD73 enzymatic activity with AB680 significantly increased gemcitabine-induced DNA damage, and treatment with a selective A2B agonist restored this phenotype. Our data support the notion that inhibitors of CD73 activity potentiate the activity of gemcitabine in PDAC. Another independent group also recently demonstrated that anti-CD73 treatment significantly improves gemcitabine efficacy against mouse KPC tumors (58). Interestingly, CD73 was shown to promote recruitment of immunosuppressive myeloid cells in a GM-CSF-dependent manner.

Because A2B receptor signaling has been shown to induce p53 activity (59), ADO production from CD73 may activate p53-mediated DNA repair mechanisms. Intriguingly, CD39 activity has also been shown to promote chemoresistance. In acute myeloid leukemia cells, inhibiting CD39 blocks mitochondrial reprogramming triggered by cytarabine, thus enhancing cytotoxicity (60). These complexities, however, need to be further investigated given prior results when examining other pathways of ADO generation and divergent impacts on DNA damage (61,62).

Accumulation of DNA damage in tumor cells can activate the pro-inflammatory cGAS-STING pathway. PDAC tumor cells are notably characterized by high expression of STING (63), and recent studies have demonstrated the therapeutic potential of STING agonists in mouse models of PDAC (64,65). We here provide evidence that CD73 expression in PDAC tumor cells inhibits activation of the cGAS-STING pathway. Deleting cGAS in mouse KPC tumor cells abrogated the therapeutic activity of AB680 *in vivo*. This suggests that activation of cGAS is a central trigger in the mechanism of CD73 inhibition in the KPC mouse model of PDAC. Although we did not evaluate the role of cGAS-STING for anti-CD39 therapy, inhibition of ADO signaling through CD39 inhibition

may also regulate cGAS-STING activation. Interestingly, activation of STING in mouse KPC tumors is characterized by a conversion of M2 to M1 tumor-infiltrating myeloid cells (65,66), a phenotype we also observed upon targeting of CD73 or CD39.

In conclusion, our study supports further evaluation of CD39 and CD73 biology in PDAC, with roles as immune checkpoints and in generating chemoresistance to gemcitabine. We demonstrated that both CD39 and CD73 significantly associate with poor clinical outcomes and suppress tumor immune surveillance against PDAC. We propose that targeting the CD39-CD73 axis will be beneficial in the context of immunologically cold tumors, such as PDAC.

## **Acknowledgments**

J.S. received research funds from the Canadian Institutes of Health Research, the Fonds de Recherche du Québec-Santé (FRQS), the Terry Fox Research Institute, the Quebec Cancer Consortium, the Chaire Jean-Guy Sabourin Research de l'Université de Montréal and Surface Oncology inc. S.T. received research funds from the FRQS and the Chaire Roger Des Groseillers en oncologie chirurgicale hépatobiliaire et pancréatique de l'Université de Montréal. SCR received research funds from the National Institute of Health (R01 DK108894; R21 CA164970 and R21 CA221702 ), Tizona Therapeutics, Emerson Collective Foundation and USA Department of Defense Award (W81XWH-16-0464).

We thank Véronique Barrès and Liliane Meunier of the Molecular Pathology core facility of the CRCHUM for performing the tissues sectioning, H&E and imaging of the slides. We thank L. Rousseau, J. Bilodeau and S. Langevin from the CHUM

Hepatopancreatobiliary cancer biobank for patient recruitment and of prospective clinical data management. We thank Dr. Louis Gaboury for his support in the generation of tissue microarrays at the Institut de recherche en immunologie et en oncologie of the Université de Montréal.



## References

1. Orth M, Metzger P, Gerum S, Mayerle J, Schneider G, Belka C, et al. Pancreatic ductal adenocarcinoma: Biological hallmarks, current status, and future perspectives of combined modality treatment approaches. *Radiat Oncol*. 2019;14:1–20.
2. Klein AP. Pancreatic cancer epidemiology: understanding the role of lifestyle and inherited risk factors. *Nat Rev Gastroenterol Hepatol*. 2021;18:493–502.
3. Neoptolemos JP, Kleeff J, Michl P, Costello E, Greenhalf W, Palmer DH. Therapeutic developments in pancreatic cancer: Current and future perspectives. *Nat Rev Gastroenterol Hepatol*. 2018;15:333–348.
4. Conroy T, Desseigne F, Ychou M, Bouché O, Guimbaud R, Bécouarn Y, et al. FOLFIRINOX versus gemcitabine for metastatic pancreatic cancer. *N Engl J Med*. 2011;364:1817–25.
5. Von Hoff DD, Ervin T, Arena FP, Chiorean EG, Infante J, Moore M, et al. Increased survival in pancreatic cancer with nab-paclitaxel plus gemcitabine. *N Engl J Med*. 2013;369:1691–703.
6. Pardoll DM. The blockade of immune checkpoints in cancer immunotherapy. *Nat Rev Cancer*. 2012;12:252–64.
7. Kabacaoglu D, Ciecieski KJ, Ruess DA, Algül H. Immune Checkpoint Inhibition for Pancreatic Ductal Adenocarcinoma: Current Limitations and Future Options. *Front Immunol* [Internet]. 2018 [cited 2021 Aug 5];0. Available from: <https://www.frontiersin.org/articles/10.3389/fimmu.2018.01878/full>
8. Bauer C, Kühnemuth B, Duewell P, Ormanns S, Gress T, Schnurr M. Prevailing over T cell exhaustion: New developments in the immunotherapy of pancreatic cancer. *Cancer Lett*. 2016;381:259–68.
9. Hosein AN, Brekken RA, Maitra A. Pancreatic cancer stroma: an update on therapeutic targeting strategies. *Nat Rev Gastroenterol Hepatol*. 2020;17:487–505.
10. Feng M, Xiong G, Cao Z, Yang G, Zheng S, Song X, et al. PD-1/PD-L1 and immunotherapy for pancreatic cancer. *Cancer Lett*. 2017;407:57–65.
11. Schmiechen ZC, Stromnes IM. Mechanisms Governing Immunotherapy Resistance in Pancreatic Ductal Adenocarcinoma. *Front Immunol* [Internet]. 2021 [cited 2022 Jan 27];11. Available from: <https://www.frontiersin.org/article/10.3389/fimmu.2020.613815>
12. Allard B, Allard D, Buisseret L, Stagg J. The adenosine pathway in immuno-oncology. *Nat Rev Clin Oncol*. 2020;17:611–629.

13. Yan A, Joachims ML, Thompson LF, Miller AD, Canoll PD, Bynoe MS. CD73 Promotes Glioblastoma Pathogenesis and Enhances Its Chemoresistance via A2B Adenosine Receptor Signaling. *J Neurosci*. 2019;39:4387–402.
14. Mittal D, Sinha D, Barkauskas D, Young A, Kalimutho M, Stannard K, et al. Adenosine 2B Receptor Expression on Cancer Cells Promotes Metastasis. *Cancer Res*. 2016;76:4372–82.
15. Lan J, Lu H, Samanta D, Salman S, Lu Y, Semenza GL. Hypoxia-inducible factor 1-dependent expression of adenosine receptor 2B promotes breast cancer stem cell enrichment. *Proc Natl Acad Sci*. 2018;115:E9640–8.
16. Tanaka Y, Kitabatake K, Abe R, Tsukimoto M. Involvement of A2B Receptor in DNA Damage Response and Radiosensitizing Effect of A2B Receptor Antagonists on Mouse B16 Melanoma. *Biol Pharm Bull*. 2020;43:516–25.
17. Zhao J, Soto LMS, Wang H, Katz MH, Prakash LR, Kim M, et al. Overexpression of CD73 in pancreatic ductal adenocarcinoma is associated with immunosuppressive tumor microenvironment and poor survival. *Pancreatol Off J Int Assoc Pancreatol IAP AI*. 2021;21:942–9.
18. Chen Q, Pu N, Yin H, Zhang J, Zhao G, Lou W, et al. CD73 acts as a prognostic biomarker and promotes progression and immune escape in pancreatic cancer. *J Cell Mol Med*. 2020;24:8674–8686.
19. Zhou L, Jia S, Chen Y, Wang W, Wu Z, Yu W, et al. The distinct role of CD73 in the progression of pancreatic cancer. *J Mol Med*. 2019;97:803–815.
20. Sciarra A, Monteiro I, Ménétrier-Caux C, Caux C, Gilbert B, Halkic N, et al. CD73 expression in normal and pathological human hepatobiliopancreatic tissues. *Cancer Immunol Immunother CII*. 2019;68:467–78.
21. Bendell JC, Manji GA, Pant S, Lai DW, Colabella J, Berry W, et al. A phase I study to evaluate the safety and tolerability of AB680 combination therapy in participants with gastrointestinal malignancies. *J Clin Oncol*. 2020;38:TPS788-TPS788.
22. Overman MJ, LoRusso P, Strickler JH, Patel SP, Clarke SJ, Noonan AM, et al. Safety, efficacy and pharmacodynamics (PD) of MEDI9447 (oleclumab) alone or in combination with durvalumab in advanced colorectal cancer (CRC) or pancreatic cancer (panc). *J Clin Oncol*. 2018;36:4123–4123.
23. Künzli BM, Nuhn P, Enjyoji K, Banz Y, Smith RN, Csizmadia E, et al. Disordered pancreatic inflammatory responses and inhibition of fibrosis in CD39-null mice. *Gastroenterology*. 2008;134:292–305.
24. Grassi F, De Ponte Conti B. The P2X7 Receptor in Tumor Immunity. *Front Cell Dev Biol*. 2021; 9: 694831.

25. Gendoo DMA, Zon M, Sandhu V, Manem VSK, Ratanasirigulchai N, Chen GM, et al. MetaGxData: Clinically Annotated Breast, Ovarian and Pancreatic Cancer Datasets and their Use in Generating a Multi-Cancer Gene Signature. *Sci Rep.* 2019;9:1–14.
26. Wei JS, Kuznetsov IB, Zhang S, Song YK, Asgharzadeh S, Sindiri S, et al. Clinically Relevant Cytotoxic Immune Cell Signatures and Clonal Expansion of T-Cell Receptors in High-Risk MYCN-Not-Amplified Human Neuroblastoma. *Clin Cancer Res Off J Am Assoc Cancer Res.* 2018;24:5673–84.
27. Jiang P, Gu S, Pan D, Fu J, Sahu A, Hu X, et al. Signatures of T cell dysfunction and exclusion predict cancer immunotherapy response. *Nat Med.* 2018;24:1550–8.
28. Hänzelmann S, Castelo R, Guinney J. GSEA: gene set variation analysis for microarray and RNA-seq data. *BMC Bioinformatics.* 2013;14:7.
29. Smirnov P, Safikhani Z, El-Hachem N, Wang D, She A, Olsen C, et al. PharmacoGx: an R package for analysis of large pharmacogenomic datasets. *Bioinformatics.* 2016;32:1244–6.
30. Haverty PM, Lin E, Tan J, Yu Y, Lam B, Lianoglou S, et al. Reproducible pharmacogenomic profiling of cancer cell line panels. *Nature.* 2016;533:333–7.
31. Iorio F, Knijnenburg TA, Vis DJ, Bignell GR, Menden MP, Schubert M, et al. A Landscape of Pharmacogenomic Interactions in Cancer. *Cell.* 2016;166:740–54.
32. Seashore-Ludlow B, Rees MG, Cheah JH, Cokol M, Price EV, Coletti ME, et al. Harnessing Connectivity in a Large-Scale Small-Molecule Sensitivity Dataset. *Cancer Discov.* 2015;5:1210–23.
33. Alcedo KP, Rouse MA, Jung GS, Fu D, Minor M, Willcockson HH, et al. CD73 Maintains Hepatocyte Metabolic Integrity and Mouse Liver Homeostasis in a Sex-Dependent Manner. *Cell Mol Gastroenterol Hepatol.* 2021;12:141–57.
34. Enjyoji K, Sévigny J, Lin Y, Frenette PS, Christie PD, Esch JS, et al. Targeted disruption of cd39/ATP diphosphohydrolase results in disordered hemostasis and thromboregulation. *Nat Med.* 1999;5:1010–7.
35. Rothweiler S, Feldbrügge L, Jiang ZG, Csizmadia E, Longhi MS, Vaid K, et al. Selective deletion of ENTPD1/CD39 in macrophages exacerbates biliary fibrosis in a mouse model of sclerosing cholangitis. *Purinergic Signal.* 2019;15:375–85.
36. Longati P, Jia X, Eimer J, Wagman A, Witt M-R, Rehnmark S, et al. 3D pancreatic carcinoma spheroids induce a matrix-rich, chemoresistant phenotype offering a better model for drug testing. *BMC Cancer.* 2013;13:95.
37. Borenstein M, Higgins JPT. Meta-analysis and subgroups. *Prev Sci Off J Soc Prev Res.* 2013;14:134–43.

38. Higgins JPT, Thompson SG, Deeks JJ, Altman DG. Measuring inconsistency in meta-analyses. *BMJ*. 2003;327:557–60.
39. Tang R, Liu X, Liang C, Hua J, Xu J, Wang W, et al. Deciphering the Prognostic Implications of the Components and Signatures in the Immune Microenvironment of Pancreatic Ductal Adenocarcinoma. *Front Immunol* [Internet]. 2021 [cited 2022 Jan 25];0. Available from: <https://www.frontiersin.org/articles/10.3389/fimmu.2021.648917/full#h5>
40. Lohneis P, Sinn M, Bischoff S, Jühling A, Pelzer U, Wislocka L, et al. Cytotoxic tumour-infiltrating T lymphocytes influence outcome in resected pancreatic ductal adenocarcinoma. *Eur J Cancer Oxf Engl* 1990. 2017;83:290–301.
41. Kwon J, Bakhoum SF. The Cytosolic DNA-Sensing cGAS–STING Pathway in Cancer. *Cancer Discov*. 2020;10:26–39.
42. Ballehaninna UK, Chamberlain RS. The clinical utility of serum CA 19-9 in the diagnosis, prognosis and management of pancreatic adenocarcinoma: An evidence based appraisal. *J Gastrointest Oncol*. 2012;3:105–19.
43. Rittmann MC, Hussung S, Braun LM, Klar RFU, Biesel EA, Fichtner-Feigl S, et al. Plasma biomarkers for prediction of early tumor recurrence after resection of pancreatic ductal adenocarcinoma. *Sci Rep*. 2021;11:1–12.
44. Turiello R, Capone M, Giannarelli D, Morretta E, Monti MC, Madonna G, et al. Serum CD73 is a prognostic factor in patients with metastatic melanoma and is associated with response to anti-PD-1 therapy. *J Immunother Cancer*. 2020;8:e001689.
45. Messaoudi N, Cousineau I, Arslanian E, Henault D, Stephen D, Vandenbroucke-Menu F, et al. Prognostic value of CD73 expression in resected colorectal cancer liver metastasis. *Oncoimmunology*. 2020;9:1746138.
46. Klemens MR, Sherman WR, Holmberg NJ, Ruedi JM, Low MG, Thompson LF. Characterization of soluble vs membrane-bound human placental 5'-nucleotidase. *Biochem Biophys Res Commun*. 1990;172:1371–7.
47. Vogel M, Kowalewski H, Zimmermann H, Hooper NM, Turner AJ. Soluble low-Km 5'-nucleotidase from electric-ray (*Torpedo marmorata*) electric organ and bovine cerebral cortex is derived from the glycosyl-phosphatidylinositol-anchored ectoenzyme by phospholipase C cleavage. *Biochem J*. 1992;284 ( Pt 3):621–4.
48. Fini C, Talamo F, Cherri S, Coli M, Floridi A, Ferrara L, et al. Biochemical and mass spectrometric characterization of soluble ecto-5'-nucleotidase from bull seminal plasma. *Biochem J*. 2003;372:443–51.
49. Kalsi K, Lawson C, Dominguez M, Taylor P, Yacoub MH, Smolenski RT. Regulation of ecto-5'-nucleotidase by TNF-alpha in human endothelial cells. *Mol Cell Biochem*. 2002;232:113–9.

50. Li X-Y, Moesta AK, Xiao C, Nakamura K, Casey M, Zhang H, et al. Targeting CD39 in Cancer Reveals an Extracellular ATP- and Inflammasome-Driven Tumor Immunity. *Cancer Discov.* 2019;9:1754–73.
51. Yan J, Li X-Y, Roman Aguilera A, Xiao C, Jacobberger-Foissac C, Nowlan B, et al. Control of Metastases via Myeloid CD39 and NK Cell Effector Function. *Cancer Immunol Res.* 2020;8:356–67.
52. Moodley D, Carneiro M, Gas SD, Dulak A, Masia R, Koseoglu S, et al. Abstract 1802: CD39 inhibition shapes the transcriptional landscape of myeloid cells and induces proinflammatory states in the CT26 syngeneic tumor model. *Cancer Res.* 2021;81:1802–1802.
53. Hu C, Ding H, Li Y, Pearson JA, Zhang X, Flavell RA, et al. NLRP3 deficiency protects from type 1 diabetes through the regulation of chemotaxis into the pancreatic islets. *Proc Natl Acad Sci.* 2015;112:11318–23.
54. Romero JM, Grünwald B, Jang G-H, Bavi PP, Jhaveri A, Masoomian M, et al. A Four-Chemokine Signature Is Associated with a T-cell-Inflamed Phenotype in Primary and Metastatic Pancreatic Cancer. *Clin Cancer Res Off J Am Assoc Cancer Res.* 2020;26:1997–2010.
55. Sadej R, Spychala J, Skladanowski AC. Expression of ecto-5'-nucleotidase (eN, CD73) in cell lines from various stages of human melanoma. *Melanoma Res.* 2006;16:213–222.
56. Rust S, Guillard S, Sachsenmeier K, Hay C, Davidson M, Karlsson A, et al. Combining phenotypic and proteomic approaches to identify membrane targets in a 'triple negative' breast cancer cell type. *Mol Cancer.* 2013;12:11.
57. Yu X, Liu W, Wang Z, Wang H, Liu J, Huang C, et al. CD73 induces gemcitabine resistance in pancreatic ductal adenocarcinoma: A promising target with non-canonical mechanisms. *Cancer Lett.* 2021;519:289–303.
58. King RJ, Shukla SK, He C, Vernucci E, Thakur R, Attri KS, et al. CD73 induces GM-CSF/MDSC-mediated suppression of T cells to accelerate pancreatic cancer pathogenesis. *Oncogene.* 2022;41:971–82.
59. Long JS, Crighton D, O'Prey J, Mackay G, Zheng L, Palmer TM, et al. Extracellular adenosine sensing-a metabolic cell death priming mechanism downstream of p53. *Mol Cell.* 2013;50:394–406.
60. Aroua N, Boet E, Ghisi M, Nicolau-Travers M-L, Saland E, Gwilliam R, et al. Extracellular ATP and CD39 Activate cAMP-Mediated Mitochondrial Stress Response to Promote Cytarabine Resistance in Acute Myeloid Leukemia. *Cancer Discov.* 2020;10:1544–65.
61. Whitley MJ, Suwanpradid J, Lai C, Jiang SW, Cook JL, Zelac DE, et al. ENTPD1 (CD39) Expression Inhibits UVR-Induced DNA Damage Repair through Purinergic Signaling and Is

Associated with Metastasis in Human Cutaneous Squamous Cell Carcinoma. *J Invest Dermatol*. 2021;141:2509–20.

62. Kitabatake K, Kaji T, Tsukimoto M. Involvement of CD73 and A2B receptor in radiation-induced DNA damage response and cell migration in human glioblastoma A172 cells. *Biol Pharm Bull*. 2020;advpub.
63. Baird JR, Friedman D, Cottam B, Dubensky TW, Kanne DB, Bambina S, et al. Radiotherapy Combined with Novel STING-Targeting Oligonucleotides Results in Regression of Established Tumors. *Cancer Res*. 2016;76:50–61.
64. Jing W, McAllister D, Vonderhaar EP, Palen K, Riese MJ, Gershan J, et al. STING agonist inflames the pancreatic cancer immune microenvironment and reduces tumor burden in mouse models. *J Immunother Cancer*. 2019;7:115.
65. Ager CR, Boda A, Rajapakshe K, Lea ST, Di Francesco ME, Jayaprakash P, et al. High potency STING agonists engage unique myeloid pathways to reverse pancreatic cancer immune privilege. *J Immunother Cancer*. 2021;9.
66. Vonderhaar EP, Barnekow NS, McAllister D, McOlash L, Eid MA, Riese MJ, et al. STING Activated Tumor-Intrinsic Type I Interferon Signaling Promotes CXCR3 Dependent Antitumor Immunity in Pancreatic Cancer. *Cell Mol Gastroenterol Hepatol*. 2021;12:41–58.

**Table 1****Univariate and multivariate analysis of CD73 and CD39 association with outcomes**

<b>Univariate Analysis</b>	<b>n</b>	<b>HR (95%CI)</b>	<b>p-value</b>
Gender (male vs female)	110	0.7 (0.45-1.09)	0.117
Preoperative CA 19-9 ( $\leq 300$ vs $>300$ U/mL)	87	1.71 (1.05-2.77)	<b>0.031</b>
pN category (N0 vs N+)	110	1.83 (1.09-3.07)	<b>0.022</b>
Lymphovascular invasion (no vs yes)	97	1.77 (0.85-3.69)	0.129
Resection margin (negative vs positive)	110	1.59 (0.93-2.72)	0.09
CD73 tumoral expression (low vs high - top tertile)	104	2.61 (1.65-4.11)	<b>&lt;0.001</b>
CD73 tumoral expression (continuous variable)	104	2.11 (0.99-4.5)	0.054
CD39 stromal expression (low vs high - top tertile)	109	1.63 (1.03-2.56)	<b>0.036</b>
CD39 stromal expression (continuous variable)	109	4.03 (0.95-17.08)	<b>0.059</b>
CD8 tumoral expression (low vs high - opt.cut-point)	110	0.53 (0.32-0.88)	<b>0.015</b>
CD8 tumoral expression (continuous variable)	110	0.76 (0.51-1.14)	0.181
<hr/>			
<b>Multivariate Analysis - CD73</b>	<b>84</b>		
Preoperative CA 19-9 ( $\leq 300$ vs $>300$ U/mL)		1.77 (1.05-3)	<b>0.033</b>
pN category (N0 vs N+)		1.12 (0.6-2.09)	0.726
Differentiation (well vs moderate/poor)		1.95 (1.1-3.43)	<b>0.021</b>
Resection margin (negative vs positive)		1.48 (0.71-3.06)	0.294
CD73 tumoral expression (low vs high - top tertile)		2.27 (1.33-3.86)	<b>0.003</b>
<hr/>			
<b>Multivariate Analysis - CD39</b>	<b>86</b>		
Preoperative CA 19-9 ( $\leq 300$ vs $>300$ U/mL)		1.75 (1.02-2.99)	<b>0.041</b>
pN category (N0 vs N+)		1.08 (0.56-2.1)	0.820
Differentiation (well vs moderate/poor)		2.26 (1.3-3.93)	<b>0.004</b>
Resection margin (negative vs positive)		1.29 (0.64-2.63)	0.476
CD39 tumoral expression (low vs high - top tertile)		1.29 (0.76-2.19)	0.350
<hr/>			
<b>Multivariate - CD73 - CD39</b>	<b>83</b>		
Preoperative CA 19-9 ( $\leq 300$ vs $>300$ U/mL)		1.81 (1.06-3.06)	<b>0.028</b>
pN category (N0 vs N+)		1.17 (0.62-2.22)	0.630
Differentiation (well vs moderate/poor)		1.74 (0.97-3.1)	0.061
Resection margin (negative vs positive)		1.38 (0.66-2.89)	0.393
CD73 tumoral expression (low vs high - top tertile)		2.55 (1.47-4.41)	<b>0.001</b>
CD39 stromal expression (low vs high - top tertile)		1.46 (0.84-2.52)	0.179
<hr/>			
<b>Serology cohort Univariate Analysis</b>			
Gender (male vs female)	238	1.1 (0.83-1.46)	0.509
Preoperative CA 19-9 ( $\leq 300$ vs $>300$ U/mL)	222	1.65 (1.21-2.24)	<b>0.001</b>
pN category (N0 vs N+)	161	2.57 (1.7-3.88)	<b>&lt;0.001</b>
Differentiation (well vs moderate/poor)	151	1.6 (1.09-2.33)	<b>0.016</b>
Resection margin (negative vs positive)	238	1.84 (1.12-3.02)	<b>0.016</b>
sCD73 expression (low vs high - top quartile)	238	1.45 (1.06-1.97)	<b>0.020</b>
sCD73 expression (continuous variable)	238	1.02 (1.00-1.04)	<b>0.027</b>
<hr/>			
<b>Serology cohort Multivariate Analysis</b>	<b>137</b>		
Preoperative CA 19-9 ( $\leq 300$ vs $>300$ U/mL)		1.34 (0.85-2.11)	0.210
pN category (N0 vs N+)		1.99 (1.26-3.16)	<b>0.003</b>

Differentiation (well vs moderate/poor)	1.51 (0.97-2.35)	0.066
Resection margin (negative vs positive)	1.46 (0.86-2.49)	0.158
CD73 tumoral expression (low vs high - top quartile)	1.43 (0.91-2.25)	0.116

Abbreviations: n, number; HR, Hazard ratio; CI, Confidence interval; CA 19- 9, Cancer antigen 19-9; T, Tumor; N, Node; CD, Cluster of differentiation



### **Figure Legends**

**Figure 1. CD73 gene expression is associated with poor PDAC prognosis. (A)** Meta-analysis of CD73 gene expression (median) with 5-year overall survival (5-y OS). Forest plot displays the log hazard ratios (logHR) and 95% confidence intervals (CI). Horizontal bars represent the 95% CI of effect-size. Blue diamond represents the overall effect in all PDAC patients. **(B)** Association between CD73 gene expression (median) and OS in CD39-High PDAC (CD73 Low: n=37; CD73 High: n=36) and CD39-Low PDAC (CD73 Low: n=37; CD73 High: n=36) from the TCGA cohort. **(C)** Spearman correlation heatmap between *ENTPD1* (CD39), *NT5E* (CD73), *PDCD1* (PD-1), *LAG3*, *CTLA4*, *TIGIT* and three signatures (CYT, CD8, and Treg) in 179 PDAC patients from the TCGA cohort. Cells are colored according to Spearman's correlation coefficient values, with blue indicating a positive correlation and red indicating a negative correlation.

**Figure 2. Tumor CD73 and stromal CD39 protein expression associate with poor PDAC prognosis and suppressed immune surveillance. (A-B)** Representative immunofluorescence staining of CD73 expression in epithelium (A) and CD39 expression in stroma (B) of PDAC tumors. Epithelium was determined as the compartment expressing cytokeratin (CK, green). Stroma is the CK-negative compartment. CD73, red; DAPI, blue. **(C-D)** Mean fluorescence intensity (MFI) of epithelial and stromal CD73 (C) and CD39 (D) expression in 104 normal adjacent pancreas (N) versus intratumoral compartment (IT) (red bars indicate mean). **(E-F)** Association between CD73 expression in tumor epithelium (CD73 Low: n=69; CD73 High: n=35) (E) or CD39 expression in tumor stroma (CD39 Low: n=73; CD39 High: n=36) (F) with overall survival (OS), using the upper tertile as cut-off. **(G-H)** Combined

prognostic value of CD8 infiltration with CD73 protein expression in epithelial tissue (G) (CD73\_Low/CD8\_Low: n=13; CD73\_Low/CD8\_High: n=55; CD73\_High/CD8\_Low: n=8; CD73\_High/CD8\_High: n=28) or CD39 protein expression in tumor stroma (H) with OS. Patients were stratified into four groups depending on expression, using upper tertile as cut-off for CD73 and CD39 and upper-quartile for CD8 (CD39 Low/CD8 Low: n=16; CD39 Low/CD8 High: n=56; CD39 High/CD8 Low: n=4; CD39 High/CD8 High: n=33) (I) Soluble CD73 (sCD73) in the serum of healthy patients (n=10) compared to patients with benign hepato-biliary disease (n=10) or PDAC patients (n=248)(median, interquartile range and 95%CI are shown). (J) Association between sCD73 and patient outcomes (Low: n=178; High: n=60), using upper quartile as a cut-off. Statistical significance was determined with Student T test (C-D), Log-rank test (E-H, J) or Wilcoxon rank-sum test (I). \*P<0.05, \*\*P<0.01, \*\*\*P<0.001, ns: not significant.

**Figure 3. CD73 on tumor cells and myeloid cells promotes mouse PDAC. (A)** CD73-positive (pos) or -negative (neg) KPC tumor cells were injected s.c. into C57BL/6 mice and treated with gemcitabine (gem; i.p. 100 mg/kg) on days 5 and 8. Mean tumor sizes are shown  $\pm$  SEM (n=9-11). **(B)** KPC tumors were analyzed at day 11 by qPCR for expression of selected immune genes. Data represent mean relative expression  $\pm$  SEM compared to CD73-positive tumors. **(C)** KPC tumors were analyzed at day 11 by FACS to assess the proportion of CD11b<sup>+</sup>Ly6G<sup>-</sup>Ly6C<sup>lo/-</sup> cells (TAMs) expressing CD206. Data represent individual and mean frequencies of TAM  $\pm$  SEM gated on CD45<sup>+</sup> cells. **(D-E)** CD73-negative KPC tumor cells were injected s.c. into CD73<sup>fl/fl</sup> LysMCre<sup>-/-</sup> mice (n=9) and into CD73<sup>fl/fl</sup> LysMCre<sup>+/-</sup> mice (n=12). On day 11, tumors were weighed (D) and the proportion of CD206<sup>+</sup> TAMs was assessed by FACS. Data are representative of 2

independent experiments (n=9-10/group). Statistical comparisons were performed using one-way ANOVA comparing indicated groups (A, C), multiple t-test or unpaired t-test (B, D, E). \*P<0.05, \*\*P<0.01, \*\*\*P<0.001, ns: not significant.

**Figure 4. CD39 cooperates with CD73 to promote mouse PDAC. (A)** KPC tumor cells were injected s.c. into CD39<sup>fl/fl</sup> LysMCre<sup>-/-</sup> mice and CD39<sup>fl/fl</sup> LysMCre<sup>+/-</sup> mice. Mean tumor sizes are shown  $\pm$  SEM (n=10). **(B-C)** KPC tumors from CD39<sup>fl/fl</sup> and LysMCre<sup>+/-</sup> CD39<sup>fl/fl</sup> mice were analyzed by FACS at day 11 to measure the proportion of CD206<sup>+</sup> TAMs and tumor-infiltrating lymphocytes (mean are shown  $\pm$  SEM). **(D)** *In vitro* spheroids composed of ovalbumin-expressing KPC (KPC-ova) and pancreatic stellate cells (WT or CD39<sup>-/-</sup>) were cultured with OT-I cells (WT or CD39<sup>-/-</sup>). The frequency of IFN- $\gamma$  producing OT-I cells was measured 8 hours later by FACS (n=3/group; means  $\pm$  SEM are shown). **(E)** Ova-expressing KPC tumors injected s.c. into C57BL/6 mice were treated with gemcitabine (i.p. 100 mg/kg, day 7 and 10) and/or anti-CD39 (i.p. 400  $\mu$ g, every three days from day 7 to 22). Mean tumor sizes  $\pm$  SEM are shown (n= 8-10). **(F)** Ova-expressing KPC tumors injected s.c. into C57BL/6 mice were treated with gemcitabine (i.p. 100 mg/kg, day 7 and 10) and/or AB680 (10 mg/kg s.c. daily from day 6 to 11). Mean tumor sizes  $\pm$  SEM are shown (n= 8-10). **(G)** Ova-expressing KPC tumors injected s.c. into CD39<sup>+/+</sup> (WT) or CD39<sup>-/-</sup> (KO) C57BL/6 mice were treated with gemcitabine (i.p. 100 mg/kg on days 6 and 9) and the CD73 inhibitor AB680 (10 mg/kg s.c. daily from day 6 to 11). Survival of mice shown. **(H)** Ova-expressing KPC tumors injected s.c. into C57BL/6 mice were treated with AB680 (10 mg/kg s.c. daily from day 6 to 10) and/or anti-CD39 (i.p. 400  $\mu$ g, on day 3, 6 and 9). On day 11, tumors were analyzed by FACS (means  $\pm$  SEM are shown). All experiments were performed twice. Statistical comparisons were performed using Mann-Whitney test (A, E), unpaired t-test (B, D, F),

multiple T-test (C, H), or log-rank test (G). \*P<0.05, \*\*P<0.01, \*\*\*P<0.001, ns: not significant.

**Figure 5. CD73 promotes DNA damage repair and suppresses cGAS-STING activation.** **(A-B)** CD73-positive (pos) or -negative (neg) KPC and PANC1 cells were exposed to increasing concentrations of gemcitabine, and proliferation was measured using CellTiter-Glo (Promega) after 48 hours of treatment. Data represents the average relative luminescence units (RLU)  $\pm$  SEM of triplicates and is representative of 4 independent experiments. **(C)** Meta-analysis of CD73 gene association with sensitivity to gemcitabine in PDAC cell lines from the Genentech Cell Line Screening Initiative (gCSI), the Genomics of Drug Sensitivity in Cancer (GDSC), and the Cancer Therapeutics Response Portal (CTRP) datasets. Forest plot displaying the C-Index and 95% confidence intervals (CI) for each dataset. Horizontal bars represent the 95% confidence intervals of effect-size. The blue diamond represents the overall effect of the variable. **(D)** Representative images of  $\gamma$ -H2AX foci detected by immunofluorescence. **(E)** Number of  $\gamma$ -H2AX foci detected by immunofluorescence in CD73-positive or -negative KPC tumor cells following 48 hours of gemcitabine treatment at the indicated doses (n=4; mean  $\pm$  SEM). **(F)** Number of  $\gamma$ -H2AX foci over time detected by immunofluorescence in KPC tumor cells following 1 Gy irradiation (n=3; mean  $\pm$  SEM). **(G)** Number of  $\gamma$ -H2AX foci detected in human PANC1 cells treated with gemcitabine, CD73 inhibitor AB680, and/or A2B receptor agonist BAY 60-6583 (n=3; mean  $\pm$  SEM). **(H)** Number of  $\gamma$ -H2AX foci detection after 48 hours of gemcitabine treatment in KPC tumor cells, in presence or absence of BAY 60-6583 (A2B receptor agonist)(n=3; mean  $\pm$  SEM). **(I)** CD73-positive or -negative KPC tumor cells were exposed to gemcitabine (20 nM) for 48 hours and

cGAMP was measured in supernatants by ELISA (n=3; mean  $\pm$  SEM). **(J)** Following gemcitabine exposition, cGAS-induced gene expression in KPC cells was measured by qPCR (n=2; mean  $\pm$  SEM). **(K)** CD73-positive KPC tumor cells expressing cGAS or not were injected in mice (n=10 per group). Some groups were treated with AB680 (peri-tumoral, 10mg/kg daily from day 6 to 11). Means  $\pm$  SEM tumor growth at day 20 are shown (experiment performed once). Statistical significance was determined with Student T test (A-B, E-K). \*P<0.05, \*\*P<0.01, \*\*\*P<0.001, ns: not significant.

Figure 1

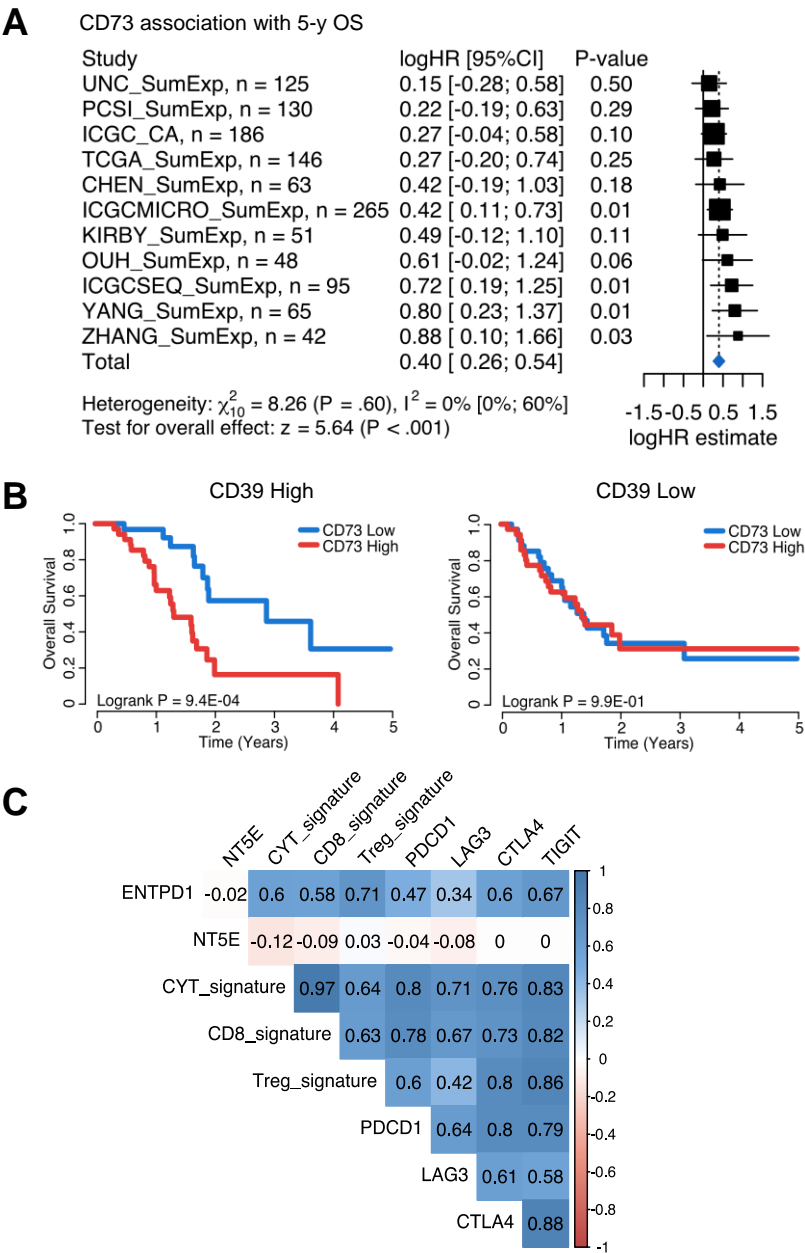


Figure 2

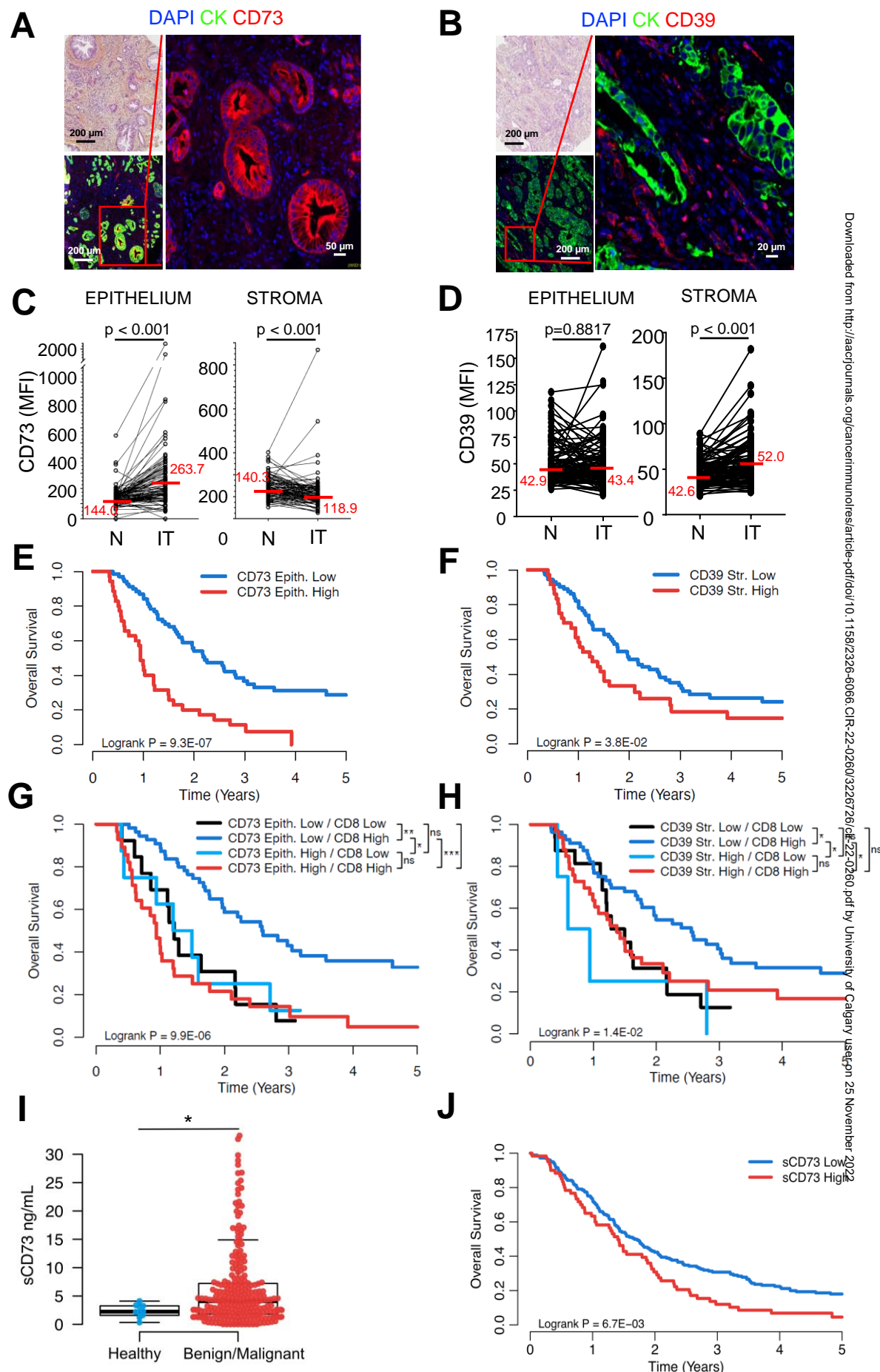


Figure 3

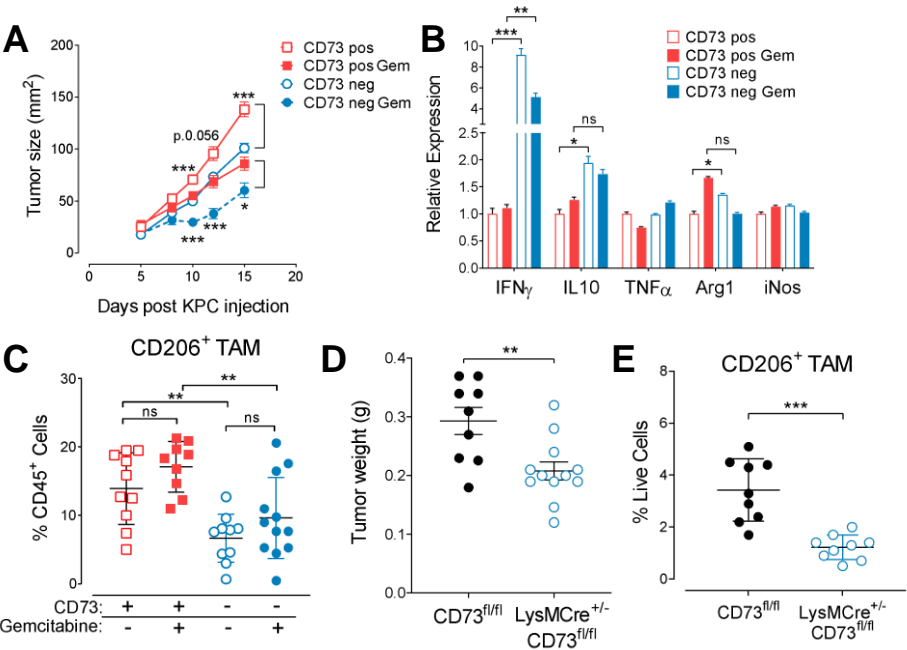




Figure 4

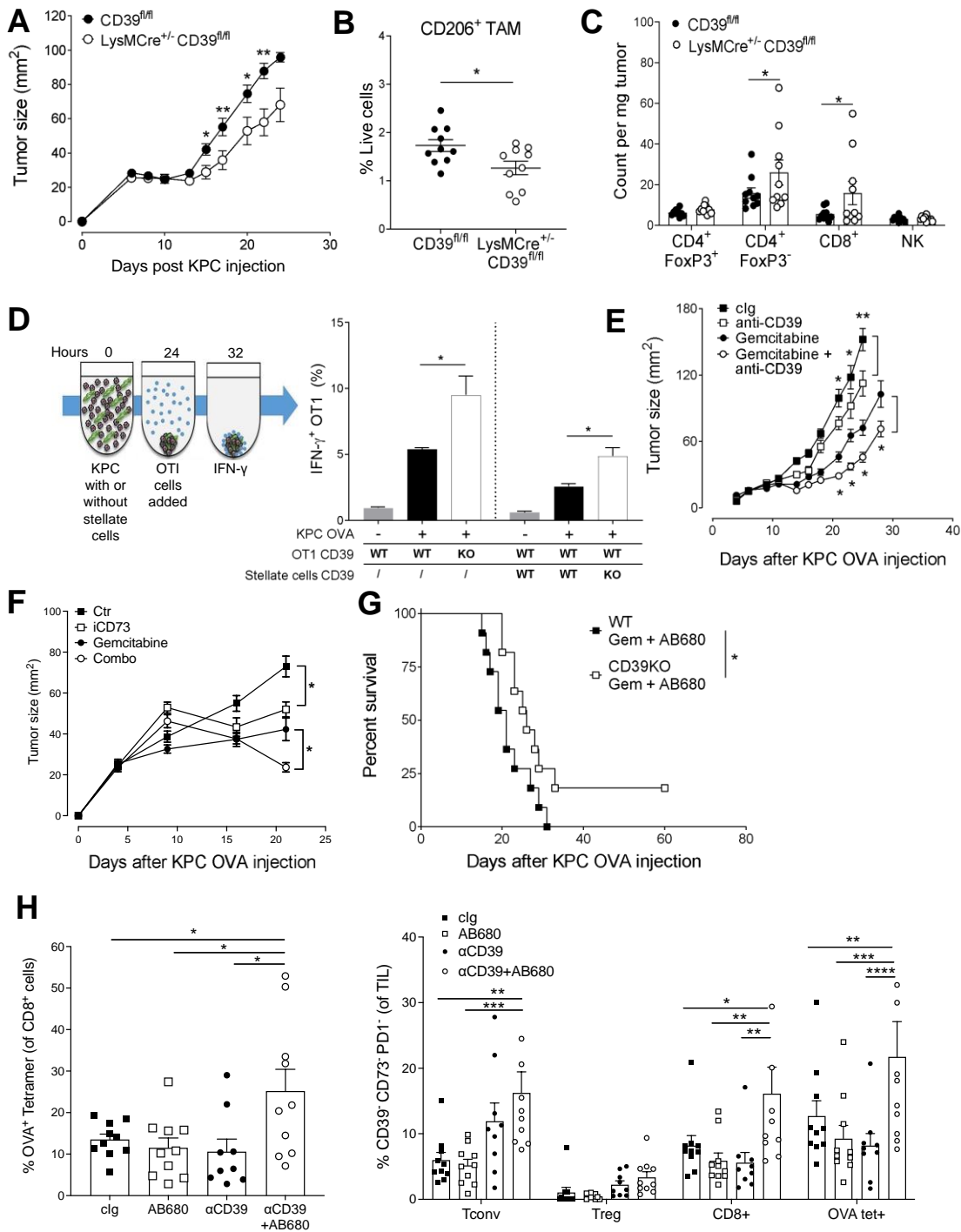
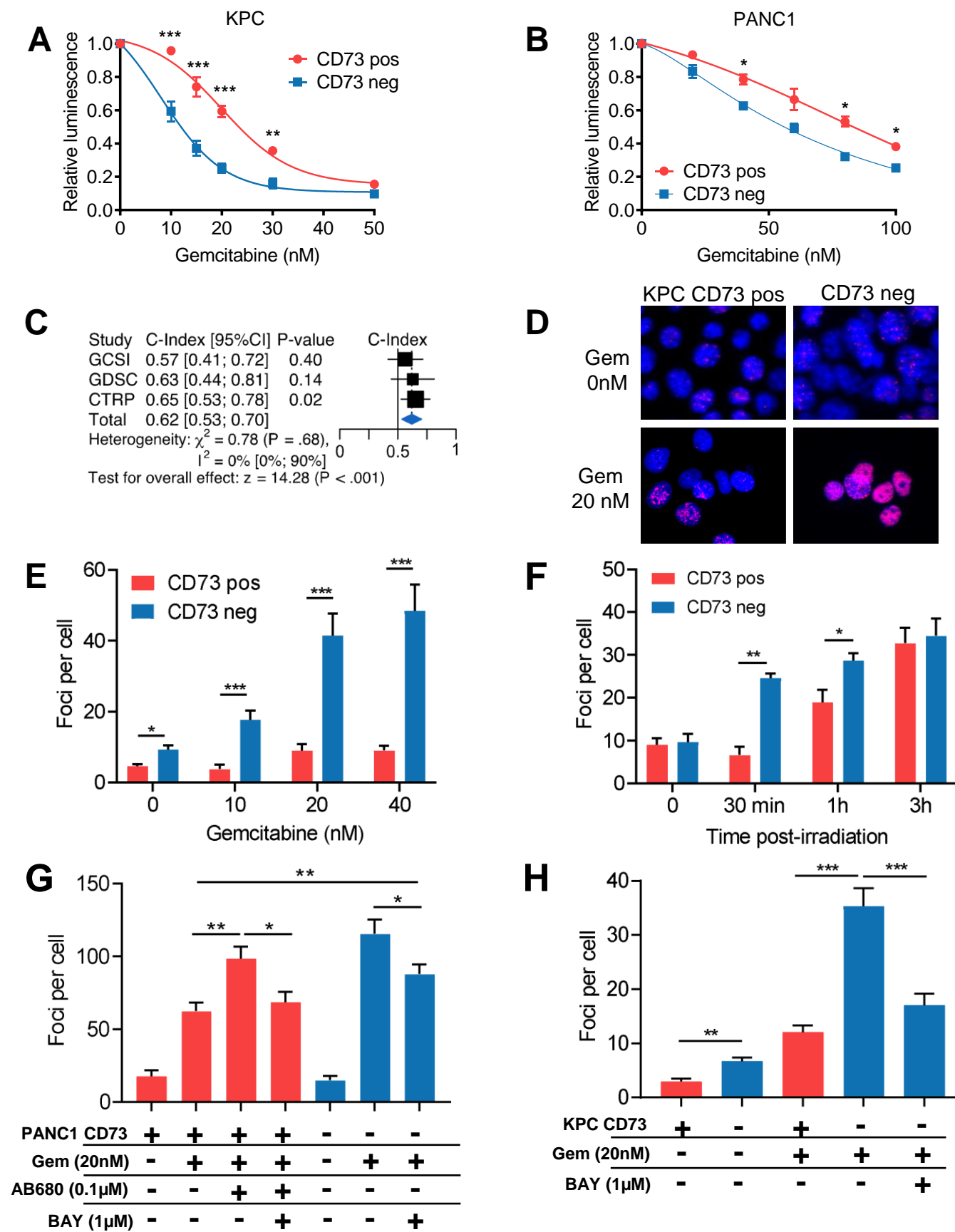


Figure 5



**Figure 5**

